Fierro, D.; Boschetti de Fierro, A.; Abetz, V.:

The Solution-Diffusion with Imperfections Model as a Method to Understand Organic Solvent Nanofiltration of Multicomponent Systems

In: Journal of Membrane Science (2012) Elsevier

DOI: 10.1016/j.memsci.2012.04.027

The Solution-Diffusion with Imperfections Model as a Method to Understand Organic Solvent Nanofiltration of Multicomponent Systems

Daniel Fierro[#], Adriana Boschetti-de-Fierro[&], Volker Abetz*

Institute of Polymer Research, Helmholtz-Zentrum Geesthacht, Max-Planck-Str. 1, 21502 Geesthacht, Germany

[#]current address: School of Engineering, Reutlingen University, Alteburgstrasse 150, 72762 Reutlingen, Germany

[&]current address: Gambro Dialysatoren GmbH, Research and Development, Holger-Crafoord-Str. 26, 72379 Hechingen, Germany

*corresponding author: volker.abetz@hzg.de

Abstract

The solution-diffusion with imperfections model has been used together with diffusion models such as the Vrentas & Duda diffusion theory and the Wesselingh & Bollen multicomponent diffusion model as a tool to successfully describe the permeation behavior of mixtures of ketones and glycols through polydimethylsiloxane composite membranes in a cross-flow membrane cell for pressures varying from 10 to 40 bar. The model has shown the great importance of an accurate determination of the diffusion coefficients and the average concentration of permeants inside the membrane into the successful modeling of nanofiltration experiments.

Keywords: Organic solvent nanofiltration, solution-diffusion with imperfections model, diffusion theory, diffusion through polymer matrix, multicomponent diffusion.

1. Introduction

Nanofiltration processes that use solvent resistant membranes have gained an important place in chemical technology and are used in a broad range of applications [1]. The use of an increasing amount of solvents in a variety of industrial processes and the deficiencies associated to classical separation techniques stimulate the development of efficient separation techniques which reduce the associated cost of materials and benefit the environment with lower energy consumption and higher recovery of residual substances than those associated to

the classical ones. Among the most promising new technologies for separating organic substances are processes based on solvent resistant nanofiltration membranes (SRNF) [2-6]. Those membrane based processes have gained an important place in the chemical, food, petrochemical and pharmaceutical industries by improving catalyst recovery, comestible oil purification, fractionation of petroleum products or separation of peptides and antibiotics, respectively. For the establishment and improvement of organic solvent separation processes in the industry, it is necessary to develop nanofiltration membranes with an ideal condition of high permeability and high selectivity. The use of a reliable transport model facilitates the optimizations of the processes before, during and after the separation itself [7-11].

For the above mentioned development of nanofiltration membranes, as well as for the improvement of the associated processes, a mathematic description and comprehension of the variables which affect the transport mechanism in nanofiltration processes is necessary. In order to describe transport through nanofiltration membranes, approaches like solution-diffusion model, Spiegler-Kedem model, Machado's resistances model, pore flow model, and solution-diffusion with imperfections model have been extensively used, with different levels of success [1]. For traditional membrane based separation processes where one substance is permeated through the membrane and the other is rejected by the membrane, the affinity between the permeant and the polymer of the membrane plays a key role during the separation process [12]. This affinity affects the swelling of the polymer and the movement capacity of the permeant inside the membrane, and both variables affect the final behavior of the membrane. This is especially true for organic solvent nanofiltration where permeation of both feed substances will occur [1, 13, 14].

A more complicated situation arises when the affinity between the permeants and the polymer membrane can no longer be considered as identical. In such a case, the permeants behave as a nonideal mixture, and the interaction between each component in the system needs to be considered in the modeling of the transport mechanism, i.e., interaction between the permeants and the interaction of each permeant with the membrane. By considering the permeants as non-ideal mixtures, the applications of the modeling loose restrictions and come closer to diverse industrial applications. Although the solution-diffusion model [15-17] and more recently the solution-diffusion with imperfections model [18] have been used to describe the permeation behavior of organic molecules through polymeric membranes, the swelling of the polymeric membrane, the interaction between the permeants as well as the

diffusion coefficients of each of them continue to be a wide research area due to the key role those parameters play into the nanofiltration process [8, 14, 19-23].

In a first paper, tracer diffusion coefficients were modeled based on two different methods, the Vrentas & Duda diffusion theory and the Wesselingh & Bollen multicomponent diffusions model [24]. Both approaches were contrasted with experimental diffusivity data obtained from PFG-NMR measurements with the aim to obtain reliable data to be used in the here employed transport model. The present work focuses on the validation of the solution-diffusion with imperfections model as a transport mechanism theory of nanofiltration processes when a non-ideal mixture permeates through the membrane. Thus, the permeation of mixtures of ketones and glycols through a dense polydimethylsiloxane (PDMS) membrane (developed by the Helmholtz-Zentrum Geesthacht) were investigated with the ultimate vision of moving forward to a general modeling for the nanofiltration industrial processes.

2. Membrane separation processes

2.1 Pore–flow model

The transport mechanism through porous membranes is based on the pore–flow model. The principle of the separation process is based on size exclusion. The starting point for the mathematical description of permeation in all membranes is that the driving forces of pressure, temperature, concentration and electromotive force are interrelated and that the overall driving force that facilitates the movement of a permeant is the gradient in its chemical potential [16]. Equation 1 represents the volumetric flux of a substance *i* (J_i) as a function of the molar concentration, the mobility or flexibility of the substance *i* when it goes through the membrane and the driving force [25].

$$J_i = -\bar{c}_i \widetilde{L}_i \frac{d\mu_i}{dz} \qquad \text{Eq. 1}$$

where $d\mu_i/dz$ is the chemical potential gradient which appears over the membrane thickness. $\widetilde{L}_i$ is a proportionality coefficient which represents the mobility of the permeant and is not necessarily constant, and $\bar{c}_i$ is the average molar concentration of the component *i*. With the consideration of driving forces that are only generated by concentration and pressure

gradients, the chemical potential can be described as presented in equation 2. c_i is the molar concentration of component i, γ_i is the activity coefficient, P is the pressure and V_i is the molar volume.

$$d\mu_i = RT\,d\ln(\gamma_i c_i) + V_i\,dP \qquad \text{Eq. 2}$$

The first assumption done in order to define any model of permeation is that the fluids on either side of membrane are in equilibrium with the membrane at the interface. Consequently, there is a continuous gradient of the chemical potential across the membrane. Additionally, the pore–flow model assumes that the concentrations of solvent and solute within a membrane are uniform and that the chemical potential gradient across the membrane can be expressed only as a pressure gradient (as shown in figure 1a). In the pore–flow model, the pressure difference produces a smooth gradient in pressure through the membrane, but the solvent activity ($\gamma_i \cdot c_i$) remains constant within the membrane [16].

When a constant solvent activity within the cross section of the membrane is considered, equations 1 and 2 can be combined and integrated over the membrane thickness in order to obtain an expression for the flux of a component i through the pores of the membrane.

$$J_i = -c_{i,F}\,\widetilde{L}_i V_i \frac{dP}{dx} \qquad \text{Eq. 3}$$

$$J_i = \frac{c_{i,F}\,k_i^{\,D}}{l\eta_i}\Delta P \qquad \text{Eq. 4}$$

where $c_{i,F}$ is the molar concentration upstream from the membrane, $k_i^{\,D}$ is the Darcy's law coefficient, and l is the thickness of the membrane. The negative sign is missing in order to show that the flux direction goes from the high pressure side to the low pressure one. The Darcy's law coefficient can be related to the pore properties of the membrane as found elsewhere [16].

2.2 Solution–diffusion model

The transport through non–porous membranes (dense membranes) is described with the solution-diffusion model [26]. For those processes, the transport mechanism implies three steps: absorption on the feed side, diffusion through the membrane and desorption on the permeate side. To be coherent with the general assumption of a continuous gradient of the chemical potential, it is implicit that the rate of absorption and desorption at the membrane interface are much higher than the rate of diffusion through the membrane. The absorption and desorption processes do not influence the overall transport rate of the molecules through the membrane, therefore, the limiting process for the permeation rate is only the diffusion of the substances through the membrane. The last considerations are no longer valid in transport involving chemical reactions or in diffusion of gases through metals, where the absorption/desorption rates are slow [17].

Contrary to the pore–flow model, the solution-diffusion model assumes that the pressure within the membrane is constant. Therefore, the chemical potential gradient across the membrane is produced only as a concentration gradient between the feed and the permeate side, as shown in figure 1b. This assumption implies that the membrane transmits the pressure in the same way as liquids do [16].

The solution-diffusion model has the same starting point as the pore–flow model, as shown in equation 1, where the flux is related with the concentration, the mobility or flexibility of the permeating molecule and the driving force expressed by the chemical potential gradient. The Nernst-Einstein equation offers a relationship between the thermodynamic diffusion coefficient (D_i) and the mobility of the permeating molecule. With the combination of equations 1, 2 and 6, the general transport equation can be written as a function of a constant diffusion coefficient as presented in equation 7.

$$D_i = \widetilde{L}_i RT \qquad \text{Eq. 6}$$

$$J_i = -\bar{c}_{i,M} D_i \left(\frac{d \ln a_i}{dz} + \frac{V_i}{RT} \frac{dP}{dz} \right) \qquad \text{Eq. 7}$$

Equation 7 can be reduced to the well known Fick's first law of diffusion when the concentration gradient is considered as the only driving force. Therefore, under the proper conditions, the thermodynamic diffusion coefficient becomes equal to the Fick's diffusion coefficient.

$$J_i = -D_i^F \left(\frac{dc_i}{dz} \right) \qquad \text{Eq. 8}$$

With the consideration of a constant pressure over the whole cross section of the membrane, the term dP/dz from equation 2 is equal to zero after the integration inside the membrane over the membrane thickness. Consequently, the flux of a component *i* can be expressed as follows:

$$J_i = -\frac{\bar{c}_{i,M} D_i}{l} \ln \left(\frac{a_{i,MP}}{a_{i,MF}} \right)$$

$$J_i = \frac{\bar{c}_{i,M} D_i}{l} \left(\ln a_{i,MF} - \ln a_{i,MP} \right) \qquad \text{Eq. 9}$$

Assuming that the feed and permeate mixtures are in equilibrium with the membrane interfaces, the chemical potential of each component outside the membrane are equal to the ones inside the membrane. Therefore, this assumption allows the estimation of the activities at the inner membrane surfaces by calculating the activities at the feed and permeate sides outside the membrane.

$$\mu_{i,F} = \mu_{i,MF}$$

$$\mu_{i,F} - \mu_i^0 = \mu_{i,MF} - \mu_i^0$$

Eq. 10

$$RT \ln a_{i,F} + V_i\left(P_F - P_o\right) = RT \ln a_{i,MF} + V_i\left(P_{MF} - P_o\right)$$

$$\xrightarrow{P_F = P_{MF}} a_{i,F} = a_{i,MF}$$

$$\mu_{i,P} = \mu_{i,MP}$$

$$\mu_{i,P} - \mu_i^0 = \mu_{i,MP} - \mu_i^0$$

$$RT \ln a_{i,P} + V_i\left(P_P - P_o\right) = RT \ln a_{i,MP} + V_i\left(P_{MP} - P_o\right)$$

Eq. 11

$$\xrightarrow{P_{MP} = P_F} RT \ln a_{i,P} = RT \ln a_{i,MP} + V_i\left(P_F - P_P\right)$$

$$\ln a_{i,P} - \frac{V_i}{RT}\Delta P = \ln a_{i,MP}$$

$$J_i = \frac{\bar{c}_{i,M} D_i}{l}\left[\ln a_{i,F} - \left(\ln a_{i,P} - \frac{V_i}{RT}\Delta P\right)\right]$$

Eq. 12

~~Equation 7 can be integrated in the outer membrane surfaces obtaining an identical result as shown in equation 12. To achieve this result, it is not necessary to consider a constant pressure over the cross section of the membrane. The pressure inside the membrane can be considered as a linear gradient; therefore, the most controversial assumption of the solution-diffusion model (i.e., constant pressure inside the membrane) vanishes, as shown in figure 1c.~~

$$\int_0^l J_i dz = -\bar{c}_{i,M} D_i \left(\int_{a_{i,F}}^{a_{i,P}} d\ln a_i + \frac{V_i}{RT} \int_{P_F}^{P_P} dP \right)$$

$$J_i l = -\bar{c}_{i,M} D_i \left(\ln \frac{a_{i,P}}{a_{i,F}} + \frac{V_i}{RT} \Delta P \right)$$

$$J_i l = -\bar{c}_{i,M} D_i \frac{V_i}{RT} \left((P_P - P_F) + \frac{RT}{V_i} \ln \frac{a_{i,P}}{a_{i,F}} \right)$$

$$J_i = \frac{\bar{c}_{i,M} D_i}{l} \frac{V_i}{RT} \left(\Delta P + \frac{RT}{V_i} \ln \frac{a_{i,F}}{a_{i,P}} \right)$$

Eq. 13

2.3 Concentration inside the membrane

The concentration inside the membrane can be estimated with the Flory-Huggins-Staverman (FHS) theory for ternary systems after the consideration presented in equation 10, as follows:

$$\ln a_{1,F} = \ln \phi_{1,M} + (1 - \phi_{1,M}) - \frac{V_1}{V_2} \phi_{2,M} - \frac{V_1}{V_3} \phi_{3,M} + \ldots$$

$$(\chi_{12} \phi_{2M} + \chi_{13} \phi_{3M})(\phi_{2M} + \phi_{3M}) - \chi_{23} \frac{V_1}{V_2} \phi_{2M} \phi_{3M}$$

Eq. 13

$$\ln a_{2,F} = \ln \phi_{2,M} + (1 - \phi_{2,M}) - \frac{V_2}{V_1} \phi_{1,M} - \frac{V_2}{V_3} \phi_{3,M} + \ldots$$

$$\left(\chi_{12} \phi_{1M} \frac{V_2}{V_1} + \chi_{23} \phi_{3M} \right)(\phi_{1M} + \phi_{3M}) - \chi_{13} \frac{V_2}{V_1} \phi_{1M} \phi_{3M}$$

Eq. 14

$$\phi_{1M} + \phi_{2M} + \phi_{3M} = 1$$

Eq. 15

The parameters $a_{1,F}$ and $a_{2,F}$ represent the activity coefficient of each solvent in a binary mixture outside the membrane (feed and permeate solution). These parameters are easily calculated with the UNIFAC method by knowing the composition of the feed solution, while the FHS interaction parameters in the ternary system solvent–solvent–membrane can be estimated by the use of swelling experiments [27-30]. By definition, when the equilibrium is

reached in the swelling experiments, the activity coefficients of each solvent inside the membrane should be identical to the one in the binary solution outside the polymer, as schematically shown in figure 2. Therefore, by applying equations 13 to 15 to the swelling experiments, the FHS parameters are calculated through the activity coefficients calculated from the binary solutions. Later, those interaction parameters facilitate the estimation of the real solvent concentration inside the membrane for the feed and permeate conditions.

2.4 Mutual diffusion coefficient

Together with the concentration of the permeants inside the membrane, the mutual diffusion coefficients are vital for the analysis of many polymer processing operations [31]. The term tends to be confusing for mixtures of superior order, therefore, it is often called thermodynamic or Maxwell-Stefan diffusion coefficient.

In order to obtain an expression for the mutual diffusion coefficients, an expression which relates the self-friction coefficient is needed. Unfortunately, there appears to be no appropriate theory which can be readily evaluated to produce an expression which relates the self-friction factors between each other in polymer–solvent systems [19, 31]. A common assumption is to consider that the mutual coefficients are the geometrical average of the two corresponding self-coefficients, as shown in equation 16.

$$\zeta_{i,j\forall i\neq j} = \sqrt{\zeta_{i\#,i}\zeta_{j\#,j}} \qquad \text{Eq. 16}$$

Hence, the mutual diffusion coefficient for a binary polymer–solvent system can be determined as follows [32-34]:

$$D = \breve{D}_1\left(1-\phi_1\right)^2\left(1-2\chi\phi_1\right) \qquad \text{Eq. 17}$$

For most of the engineering and membrane processes where diffusion plays a key role, equation 17 can be applied. However, for middle-high permeant concentration as well as multicomponent mixtures, additional parameters – which need to be fitted from experimental diffusion data – have to be included in order to describe the mutual diffusivities of the system.

The above mentioned equations to estimate the binary diffusion coefficients cannot be easily extended for ternary systems without the introduction of unknown parameters which need to be adjusted from experimental data. To achieve the extension for ternary systems, Wesselingh & Bollen consider that the effective tracer friction coefficients are linearly related with the self-diffusion friction coefficients, as shown in equation 18. Therefore, it is considered that the tracer friction coefficients have a low concentration dependence, so they do not influence each other [19].

$$\zeta_{i\#,eff} = x_i \zeta_{i\#i} + \sum_{\forall j \neq i} x_j \zeta_{i\#,j} \qquad \text{Eq. 18}$$

By introducing equation 16 into equation 18, and after proper reorganization, the mutual friction coefficients for ternary solvent–solvent–polymer systems can be calculated by equation 19.

$$\zeta_{ij} = \frac{\zeta_{i\#,eff}\ \zeta_{j\#,eff}}{\sum_k x_k \zeta_{k\#,eff}} \quad \forall i \neq j \qquad \text{Eq. 19}$$

where ζ_{ij} represents the mutual diffusion coefficient and the summation is done over the whole number of components. The mutual diffusion coefficient is estimated with equation 20.

$$D_{ij} = \frac{RT}{\zeta_{ij}} \quad \forall i \neq j \qquad \text{Eq. 20}$$

2.5 Compaction factor

In the majority of composite membranes under high pressure, a falling rate behavior of the permeation flux with the increase of pressure is found [35, 36]. Different ways to account for this effect have been proposed. On one hand, Paul et al. describes a concentration gradient induced by the applied pressure and a falling diffusion caused by it [23, 36-38]. On the other hand, Machado et al. explained this performance by the fact that the majority of composite membranes can compact themselves during filtration process. The consequence of this

compaction resides in a decrease of the membrane thickness with the consequent reduction of the free volume inside the membrane [39, 40]. Although both approaches are extensively used in the recent literature, in this work we follow the later one.

Machado et al. described the falling behavior with the following relations (equations 21 and 22). There, L_i^0 and l_i^0 are the permeability and the membrane thickness under atmospheric pressure, respectively [39].

$$J_i = L_i^0 e^{-\alpha \Delta P} \Delta P \qquad \text{Eq. 21}$$

$$L_i^0 \sim \frac{1}{l^0}$$

$$J_i = L_i(P)\,\Delta P$$

$$L_i = \frac{1}{l} \qquad \text{Eq. 22}$$

$$l = l^0 e^{\alpha \Delta P}$$

In the presence of compaction a lower permeation flux than the one expected is found. Consequently, the flux decreases when the pressure increases, as if the selective layer were thicker than before but without any change on the free volume.

The compaction factor α is extensively related with the swelling degree of the membrane. Therefore, for a mixture of solvents, a mixing rule which describes the compaction for a broad concentration range needs to be considered [8].

$$\alpha = \sum_{\substack{i \\ \text{all comp}}} a_i \alpha_i \qquad \text{Eq. 23}$$

Here, α is the compaction factor of the membrane and α_i is the compaction factor which appears in the presence of a pure solvent *i*. In order to consider the whole contribution of the

chemical potential instead of only the one from the molar fractions, the mixing rule is taken as a function of the solvent activities instead of the molar fractions.

2.6 Solution–diffusion with imperfections model

The solution-diffusion with imperfections model was an early modification of the solution-diffusion model. Sherwood et al. postulated that the transport mechanism can be expressed as a combination of diffusion through the dense layer of the membrane and pore transport through small imperfections or defects in the membrane [41]. Therefore, the model adds a second term to the solution-diffusion model, corresponding to the possible viscous transport across the membrane, as shown in equation 24 [41-43].

$$J_i = J_{i,SDM} + J_{i,VT}$$

$$J_i = J_{i,SDM} + c_{i,F}\frac{K^*}{l\,\eta_m}\Delta P \qquad \text{Eq. 24}$$

Here, $J_{i,SDM}$ represents the flux calculated with the solution diffusion model and $J_{i,VT}$ the flux from the viscous contribution. The term K^* is a coupling coefficient describing the pore flow similar to the Darcy's law coefficient. η_m corresponds to the viscosity of the permeant mixture. Equation 24 considers that the solute concentration at the exit of an imperfection is the same as at the entrance, which is only justified with the assumption that the imperfections are nonselective. However, the imperfections are surrounded by a matrix where the solute exit-concentration is decreased. That gives rise to diffusion along the membrane which causes a concentration decrease at the exit of the imperfection. Therefore, modifications to the solution-diffusion with imperfections model have been proposed in order to consider lateral diffusion in order to balance the solute concentration at the end of the imperfections [44].

For mixtures of organic compounds with different sizes, a selectivity factor needs to be included in equation 24 in order to account for any separation discrimination between small and large molecules within the imperfections [18]. Moreover, for a general case where the imperfections are inhomogeneous, equation 24 becomes as follows:

$$J_i = J_{i,SDM} + c_{i,F}\frac{K^*\widetilde{\alpha}_l}{l\,\eta_m}\Delta P$$

$$J_i = J_{i,SDM} + c_{i,F}\frac{\widetilde{K}_i}{l\,\eta_m}\Delta P \qquad \text{Eq. 25}$$

Here, $\widetilde{\alpha}_l$ represents a selectivity factor due to the nature of the imperfections and $\widetilde{K}_i$ corresponds to the partial mechanical permeability of the imperfections. The solution-diffusion with imperfection model has shown in the past years an excellent improvement over the solution-diffusion model when permeation data for reverse-osmosis and nanofiltration membrane processes are analyzed [1, 8, 18, 45]. Nevertheless, the solution-diffusion with imperfections model has two major disadvantages. The first inconvenience is related with the partial mechanical permeability ($\widetilde{K}_i$) due to the nature of the imperfections (pores), which value is not possible to determine from the pore–flow model parameters (i.e., pore diameter, tortuosity and porosity). Therefore, for real membranes the parameter has to be found experimentally. The second disadvantage resides in the nature of the parameters which describe the diffusive flux. These parameters normally can be affected by both the concentration and the applied pressure (e.g., diffusion coefficients) with the consequent deviation between the experimental data and the calculated one [42].

3. Experimental Methods

3.1 Materials

The membrane used in this study is a composite membrane developed at the Helmholtz-Zentrum Geesthacht Centre for Materials and Coastal Research. The membrane is formed by a solvent resistant support layer made of polyacrylonitrile (PAN) and a selective top layer of a high molecular weight polydimethylsiloxane (PDMS). The PAN support was prepared by phase-inversion over a non-woven layer of poly(ethylene terephthalate) with a density of 100 g/m² and an approximated thickness of 140 µm.

The PDMS layer was coated over the PAN support with an industrial coating machine from a solution of high molecular weight PDMS, curing agent, solvent (hydrocarbon) and platinum catalyst which allows the polymer to thermally crosslink. Additionally, the membrane was crosslinked with a low energy electron beam of 150 kGy by IOM/Leipzig in order to obtain

the desired chemically resistant membrane with a PDMS layer thickness of 5 μm, as shown in figure 3.

The quality of the coating of a composite membrane is assessed by performing single gas permeation measurements of O_2 and N_2 [21]. The gas permeation was measured with a Bioblock-Scientific® soap-bubble flowmeter. The experiments were carried out with the use of a transmembrane pressure of 2.5 bar. The selectivity of the polymer/membrane is defined as the fluxes ratio between two different permeating gases as shown in equation 26.

$$\breve{\alpha}_{i/j} = \frac{Q_i}{Q_j} \qquad \text{Eq. 26}$$

where $\breve{\alpha}_{i/j}$ represents the selectivity between the gases *i* and *j*. Q represents the volumetric flow rate of the permeating gases. A defect-free PDMS composite membrane should have selectivity close to the intrinsic selectivity of the PDMS in bulk. The PDMS bulk selectivity between O_2 and N_2 varies from 2.10 to 2.15 depending on the polymer molecular weight [29, 46, 47]. Therefore, the membranes were considered free of defects when the selectivity between O_2 and N_2 was at least 2.10.

To eliminate any non-uniformity effect between the different stamps, permeation fluxes for each stamp obtained from the nanofiltration experiments were normalized by the corresponding nitrogen flux of the used stamp according to equation 27. This procedure accounts for changes in thickness, porosity and pore size distribution between the stamps.

$$J_{Norm\,k} = \frac{Q_{N_2 k}}{\overline{Q}_{N_2}} J_k \qquad \text{Eq. 27}$$

where $J_{Norm\,k}$ is the normalized flux and J_k the non-normalized one for the used stamp *k*. $Q_{N_2 k}$ and $\overline{Q}_{N_2}$ represent the nitrogen volumetric flow rate for the stamp *k* and the average one from the whole set of stamps used in this work, respectively.

Solvents with synthesis grade for diffusion and nanofiltration measurements were used as received. For the experiments with mixtures of solvents, a ketone was selected as a good permeant and a glycol as a bad one (solute). The selected ketones were ethyl methyl ketone

(MEK) and diethyl ketone (DEK). The used glycols were tetraethylene glycol (TEG), tetraethylene glycol dimethyl ether (TEGDME) and polyethylene glycol dimethyl ether 250 (PEGDME). The PEGDME was obtained from Fluka® and the rest of the solvents from MERCK®. A list of the properties of the used substances is shown in table 1. For the case of PDMS, the molecular weight of the polymer chain repeating unit is shown instead of the molecular weight of the whole polymer.

Table 1. Chemical structure and physical properties of the used substances.

Substance		CAS MERCK	*MW* (g/mol)	V_C (m³/mol)
PDMS	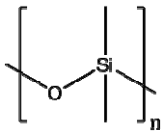	–	74.11[(a)]	–
MEK	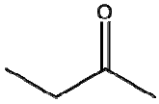	78-93-3 822253	72.11	$2.67 \cdot 10^{-4}$ [(c)]
DEK	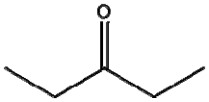	96-22-0 803605	86.13	$3.36 \cdot 10^{-4}$ [(c)]
TEGDME	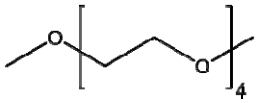	143-24-8 820959	222.28	$6.91 \cdot 10^{-4}$ [(b)]
PEGDME	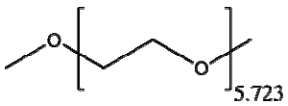	24991-55-7 814173	298.21[(b)]	$9.15 \cdot 10^{-4}$ [(b)]

(a) Molecular weight of the polymer chain repeating unit, (b) Conesa et al. [48], (c) Korea thermophysical properties data bank [49], (d) CHEM group data sheets [50]

According to Conesa et al. [48], the PEGDME 250 from Fluka® is a mixture of ethylene glycol dimethyl ethers with different chain lengths – between 3 and 9 – but is often considered as a pseudo pure compound. Therefore, a pseudo chain unit value of 5.723 was found, which corresponds to a molecular weight of 298.21 g/mol. Density and viscosity data for a range of temperatures between 10 ºC and 80 ºC were estimated for the ketones by Aspen® Custom Modeler, and the corresponding data for the glycols can be found elsewhere [48]. The density of the PDMS can be considered to be 0.970 kg/m³ for the complete range of temperatures [29].

3.2 Nanofiltration

A nanofiltration setup (figure 4) was used to investigate the effect of pressure and temperature over the filtration performance on dense membranes. The equipment is formed by a supply vessel with a recirculation cooling bath where the feed solution is kept to control its temperature. The equipment has the capability to pump the solution into the membrane cell with a relative pressure from 1 bar to 45 bar. The dead-end type membrane cell can fit a membrane with a diameter of 7.4 cm with an effective area of 37.94 cm^2 after including an o-ring which prevents any leak in the test cell. Samples from the feed, permeate and retentate solutions can be taken for the estimation of the solution concentration at those points. Hence, it is possible to take samples in the points denoted as "a", "b" and "c" in figure 4.

The pressure of the system can be regulated with an expansion valve located after the membrane cell. The temperature was changed between 20 ºC and 30 ºC in order to study the temperature effects over the permeation properties. For this, a thermostat was attached to the supply vessel and a cross-flow exchanger after the membrane cell was used. The temperature of the feed solution was controlled with the use of a digital thermometer attached at the entrance of the test cell. The membrane is left inside the membrane cell until steady-state conditions of pressure and temperature are reached. In order to achieve faster the steady-state conditions, the membranes were left overnight inside a flask with the permeation solvent allowing a pre-swelling of the membrane stamps. The permeation rate is calculated by collecting a sample of a determined volume at the point "b" of the equipment (see figure 5) and by measuring the corresponding permeation time.

To estimate the flux amount of each permeant, it is necessary to know the exact concentration of the permeated solution. In the same way, to know the final retention of the membrane during the filtration process, it is necessary to know the concentration of the feed solution. Therefore, for solutions formed by two different substances with nonsimilar densities, the average molar density can be used to calculate the concentration in a solution as shown in equation 28.

$$\rho_M = \sum_i^2 x_i \rho_i$$

Eq. 28

$$\rho_M = \rho_1 + (\rho_2 - \rho_1)\, x_2$$

To avoid any nonlinearity in the measurement, i.e., nonlinearity in the mixture density or nonlinearity in the detector, a calibration curve for a set of different concentrations was done. For the preparation of the calibration curve, solutions of 20 ml with different concentrations were prepared, i.e., from 0 wt % to 20 wt % in steps of 1 wt %. The solutions were deposited in closed glass bottles and stirred over 8 hours without heating. The curve obtained after plotting the concentration as a function of the density can be directly related with the density results from feed and permeate solutions.

The measurements have been done in a densimeter DMA 46 from Anton Paar KG. The equipment includes an integrated thermostat which keeps the temperature at the desired value. The equipment allows density estimation of organic substances when the display results are properly calibrated with water solution patterns. Due to the nature of the measurement, the calibration curve allows the calculation of solution concentrations without any further calibration of the equipment. However, a proper calibration is still needed if the exact density of the mixture is required.

4. Results and Discussion

4.1 Nanofiltration

The effect of the chain length of the permeants was investigated by comparing the permeation behavior of MEK/TEGDME and MEK/PEGDME systems. In addition, the affinity between the solvent and the polymeric membrane is studied by comparing the MEK/TEGDME and DEK/TEGDME systems. A summary of the permeation fluxes for different systems at 25 °C is shown in figures 5 to 7.

As expected, by comparing the permeation behavior of MEK/TEGDME and MEK/PEGDME (figures 5 and 6), the system with the long EGDME chain presents lower permeation fluxes than the one with the short chain length. When the MEK/TEGDME system is compared to the MEK/PEGDME system, the higher permeation observed is produced by the higher swelling degree, higher thermodynamic diffusivities and lower viscosity of the MEK/TEGDME mixture than the ones corresponding to the MEK/PEGDME system [24].

Similarly, the permeations found for the system formed by DEK/TEGDME and presented in figure 7 are higher than the corresponding ones for MEK/TEGDME (figure 5). Because the thermodynamic diffusivities for both systems are similar, the differences in permeation could be explained by the higher polymer swelling presented in the system DEK/TEGDME

compared to the one of the system MEK/TEGDME even though both systems show similar thermodynamic diffusivities [24].

The effect of temperature over the permeation behavior was investigated by MEK/TEGDME nanofiltration measurements at different temperatures (i.e., 20 ºC, 25 ºC and 30 ºC). The summary of the measurements at 20 ºC and 30 ºC is presented in figures 8 and 9, respectively, whereas the permeation at 25 ºC was previously shown in figure 5.

As shown in figures 5, 8 and 9, the permeation fluxes for both MEK and TEGDME increase when the temperature increases. This behavior is expected due to two independent contributions. First, the viscosity of any of the mixtures decreases when the temperature increases. Therefore, the viscous contribution of the permeation fluxes increases with the temperature. The second contribution refers to the increase of the polymer free volume when the temperature increases [51, 52]. This increase in the free volume of the polymer has as a consequence the increase of the diffusion coefficients, and therefore higher permeation fluxes are expected.

4.2 Modeling of organic solvent nanofiltration

For the modeling various parameters need to be known, i.e., average concentration inside the membrane and mutual diffusivities between permeants and the membrane. The molar concentration of each compound inside the membrane is calculated according by equation 28. As exemplification, a set of molar concentrations inside the membrane at different experimental conditions for the MEK/TEGDME system are summarized in table 2. Here, the concentration of PDMS increases when the TEGDME feed concentration increases, as expected from the swelling experiments previously reported [24]. Additionally, the concentration of PDMS increases when the applied transmembrane pressure increases. This behavior could be explained by the compaction of the composite membrane caused by the increment of the pressure. Therefore, when high pressures are applied, the PDMS layer is not able to increase its thickness – due to the swelling – as much as under the influence of low pressures.

Table 2. Concentration inside the membrane for the MEK/TEGDME system at different experimental conditions.

P (abs. bar)	Weight concentration in the free solution (%)		Weight concentration inside the membrane (%)			Average molar concentration (mol/m^3)		
	Feed	Permeate	S1	S2	PDMS	S1	S2	PDMS
10-40	0.00	0.00	54.2	0.0	45.8	6548.6	0.0	5376.2
10	4.72	3.73	45.1	1.9	53.0	5542.5	76.7	6347.3
20	4.76	3.10	42.1	1.7	56.2	5212.8	67.3	6765.4
30	4.86	2.69	40.2	1.6	58.2	4995.3	63.3	7035.2
40	4.77	2.40	38.8	1.5	59.7	4832.6	61.0	7234.8
10	9.89	7.86	39.2	3.7	57.1	4885.6	147.5	6921.0
20	9.97	6.60	36.9	3.2	59.9	4612.5	131.0	7292.9
30	9.78	5.69	35.3	3.0	61.7	4434.9	122.3	7528.8
40	9.85	5.05	34.1	2.9	63.0	4293.3	117.2	7711.5
10	15.21	12.22	33.7	5.1	61.2	4242.4	208.4	7505.3
20	15.12	10.55	31.8	4.5	63.7	4016.8	184.6	7843.9
30	15.13	9.02	30.5	4.1	65.4	3861.9	169.8	8070.7
40	15.05	8.09	29.4	3.9	66.6	3739.5	162.2	8237.8

"S1" corresponds to MEK and "S2" corresponds to TEGDME

The estimation of mutual diffusivities for ternary systems cannot be easily achieved without the introduction of adjustable parameters [19]. Wesselingh & Bollen proposed an easy method to estimate tracer diffusion coefficients and with the use of a mixing rule the estimation of mutual diffusivities is achieved. In this model, the success of the calculation is limited by a set of assumptions considered along the model. Therefore, the model tends to work very well on systems of similar molecules and start to fail when the components differ in size and chemical structure [8, 19, 24, 53]. The necessity of reliable data should be balanced with the increase on complexity in more general diffusion theories when the number of components in the diffusing mixture increases.

A most reliable model can be used by a combination of the most general Vrentas & Duda diffusion theory with the mixing rule from the Wesselingh & Bollen model in order to calculate the mutual diffusivities. Such approach will overcome the majority of the considerations that fail in the Wesselingh & Bollen model.

The here proposed method relies on the ability to use a few sets of experimental data from PFG-NMR measurements in order to estimate the adjustable parameters that are present in the Vrentas & Duda diffusion theory. Such adjustable parameters are intrinsic to the components and do not depend on the concentrations of those in the system. Therefore, the Vrentas & Duda theory is used to estimate tracer diffusivities of the components under the conditions presented during the permeation experiments. With such reliable values, the mixing rule proposed by Wesselingh & Bollen is applied in order to estimate the mutual diffusivities of the real system (equation 20). A scheme of the different calculation methods is presented in figure 10.

With these values, the fluxes and retentions for different ketone/EGDME nanofiltration experiments are modeled by using the solution-diffusion with imperfections model. Correlations between modeled and experimental data of the different systems here investigated are shown in figures 11 to 13, whereas the regressed parameters of the model are shown in table 3.

Table 3. Regressed parameters from the solution-diffusion with imperfections model: membrane thickness (l), partial viscous permeability of the membrane ($\widetilde{K}_i$) and compaction factor as a function of different feed concentrations (α).

Substance	l (μm)	$\widetilde{K}_i$ (10^{-10} m^2)		α (10^{-7} Pa^{-1})			
		S1	S2	0 wt %	5 wt %	10 wt %	15 wt %
MEK/TEGDME	26.6	1.99	0.36	1.70	1.39	1.22	1.01
MEK/PEGDME	50.0	1.02	0.19	1.70	1.29	1.27	1.25
DEK/TEGDME	44.4	1.44	0.88	1.16	1.12	1.02	0.92

An excellent correlation between experimental and modeled data has been found, within the errors, for all the ketone/EGDME systems, as can be appreciated in the figures 11 to 13. The estimated thickness shown in table 3 corresponds to the one of a swelled PDMS layer, which is affected by both the swelling degree and the compaction factor. For the MEK/TEGDME system, a lower thickness than the one for DEK/TEGDME is found. This tendency is expected from a comparison between the swelling degrees for both systems. Nevertheless, the estimated values of the membrane thickness are affected in both cases by the concentrations used which were obtained by the swelling experiments (i.e., concentrations inside a polymer only thermally crosslinked) instead of actual concentrations in the membrane. It is expected

that the concentration of permeants should be lower for a polymer with higher degree of crosslinking (i.e., crosslinked thermally and by radiation) than for polymers with lower degree of crosslinking (i.e., only thermally crosslinked).

Additionally, the estimated thickness for the MEK/PEGDME system is higher than the one estimated for MEK/TEGDME. This difference is not expected, since the thickness depends mainly on the swelling degree of the polymer in a given system, and this is higher in the MEK/TEGDME system than in the MEK/PEGDME system. However, this result could be explained by a higher difference in the concentration of the permeants between the thermally crosslinked polymer and the one with a further crosslinking by radiation. The difference will be higher for big molecules than for small ones due to the increased difficulty to accommodate the big molecule inside the polymer lattice when the polymer chains have less mobility.

In order to illustrate the importance of an accurate estimation of the concentration inside the membrane, the simulation results for the MEK/TEGDME system when the concentration inside the membrane is not estimated from the swelling experiments are shown in figure 14. Although a good correlation between modeled and experimental fluxes for MEK is obtained, a poor correlation is found for the TEGDME ones. For instance, the modeled results for TEGDME can differ up to 400 % from the experimental fluxes. In order to explain this behavior the effect of two different conditions on the simulated data needs to be analyzed.

The first condition is an overestimation of concentration inside the membrane for both permeants when calculated from the Flory-Huggins-Staverman theory. Since the interaction parameters are estimated only by solubility parameters for binary solutions (polymer/permeant), the presence of a second permeant inside the membrane is not considered. The second condition is that the diffusion coefficients of the good solvents are slightly overestimated and the ones corresponding to the bad solvents are underestimated when the concentration inside the membrane are calculated from the Flory-Huggins-Staverman theory for binary mixtures, as shown in our previous work [24].

In case of the good solvent, the effect of the above mentioned conditions over the modeled permeation is in some way balanced giving an apparent good correlation. In contrast, such balance does not take place in the TEGDME simulation where both the concentration and the diffusion coefficient are overestimated. Therefore, the correlation between experimental and

simulated data deviates greatly. Nevertheless, the regressed parameters for this modeling are as follows: $l = 12.7$ μm, $\widetilde{K}_{MEK} = 1.93 \cdot 10^{-10}$ m^2 and $\widetilde{K}_{TEGDME} = 7.84 \cdot 10^{-16}$ m^2.

4. Conclusions

A simulation routine to model the diffusion behavior of the components involved in nanofiltration experiments was implemented. Such routine consists of two stages where the different relevant parameters were theoretically estimated and compared to experimental measurements. First, based on reliable tracer diffusivity data of the investigated system, the Vrentas & Duda diffusion theory allows the estimation of tracer diffusivities over an extended range of concentration – namely over the range of conditions in the permeation experiments–. Second, with the use of a proper mixing rule as the one proposed by Wesselingh & Bollen, mutual diffusivities in multicomponent systems can be easily estimated.

The permeation of mixtures of ketones and glycols through dense polydimethylsiloxane composite membranes were investigated by the use of the solution-diffusion with imperfections model. The modeled permeation fluxes were directly compared with the experimental nanofiltration results in order to evaluate the quality of the simulation routine. Very good correlations were found for all ketone/glycol systems when both concentration and diffusion coefficients were estimated as previously described. Particularly, it is worth noticing the importance of a good estimation of tracer diffusion coefficient values and, even more, a precise estimation of the average concentration of the permeants inside the membrane.

A further improvement to the here presented modeling would be the use of a more general transport equation such as the Stefan–Maxwell multicomponent diffusion transport equation. Because the solution-diffusion and even more the solution-diffusion with imperfections model are based on experimental observation of the conditions presented in a nanofiltration process, the use of a general transport equation will facilitate a better understanding of industrial membrane based processes. Thus, a process development based on simulation will be facilitated.

5. Acknowledgements

The collaboration of Dr. M. F. J. Dijkstra is highly appreciated. The authors thank the German Federal Ministry of Education and Science (BMBF) for financial support via the project “Organophile Nanofiltration für die nachhaltige Produktion in der Industrie” (01R/05111).

6. References

[1] D. Bhanushali, D. Bhattacharyya, Advances in Solvent-Resistant Nanofiltration Membranes. Experimental Observations and Applications, Advanced membrane technology, 984 (2003) 159-177.

[2] J. Ducruet, K. Fast-Merlier, P. Noilet, New Application for Nanofiltration: Reduction of Malic Acid in Grape Must, Am. J. Enol. Vitic., 61 (2010) 278-283.

[3] R. Abejon, A. Garea, A. Irabien, Ultrapurification of hydrogen peroxide solution from ionic metals impurities to semiconductor grade by reverse osmosis, Sep. Purif. Technol., 76 (2010) 44-51.

[4] X.S. Li, J.E. Remias, J.K. Neathery, K.L. Liu, NF/RO faujasite zeolite membrane-ammonia absorption solvent hybrid system for potential post-combustion CO2 capture application, Journal of Membrane Science, 366 (2011) 220-228.

[5] P. Religa, A. Kowalik, P. Gierycz, Application of nanofiltration for chromium concentration in the tannery wastewater, J. Hazard. Mater., 186 (2011) 288-292.

[6] D. Peshev, L.G. Peeva, G. Peev, I.I.R. Baptista, A.T. Boam, Application of organic solvent nanofiltration for concentration of antioxidant extracts of rosemary (Rosmarinus officiallis L.), Chem. Eng. Res. Des., 89 (2011) 318-327.

[7] S. Darvishmanesh, J. Degreve, B. Van der Bruggen, Mechanisms of solute rejection in solvent resistant nanofiltration: the effect of solvent on solute rejection, Phys. Chem. Chem. Phys., 12 (2010) 13333-13342.

[8] M.F.J. Dijkstra, S. Bach, K. Ebert, A transport model for organophilic nanofiltration, Journal of Membrane Science, 286 (2006) 60-68.

[9] P. Vandezande, L.E.M. Gevers, I.F.J. Vankelecom, Solvent resistant nanofiltration: separating on a molecular level, Chem. Soc. Rev., 37 (2008) 365-405.

[10] S.U. So, L.G. Peeva, E.W. Tate, R.J. Leatherbarrow, A.G. Livingston, Organic Solvent Nanofiltration: A New Paradigm in Peptide Synthesis, Org. Process Res. Dev., 14 (2010) 1313-1325.

[11] B. Cuartas-Uribe, M.C. Vincent-Vela, S. Alvarez-Blanco, M.I. Alcaina-Miranda, E. Soriano-Costa, Application of nanofiltration models for the prediction of lactose retention using three modes of operation, J. Food Eng., 99 (2010) 373-376.

[12] S. Sourirajan, Separation of Hydrocarbon liquids by flow under pressure through porous membranes, Nature, 203 (1964).

[13] D. Bhanushali, S. Kloos, D. Bhattacharyya, Solute transport in solvent-resistant nanofiltration membranes for non-aqueous systems: experimental results and the role of solute-solvent coupling, Journal of Membrane Science, 208 (2002) 343-359.

[14] J.A. Whu, B.C. Baltzis, K.K. Sirkar, Nanofiltration studies of larger organic microsolutes in methanol solutions, Journal of Membrane Science, 170 (2000) 159-172.

[15] H.K. Lonsdale, U. Merten, R.L. Riley, Transport properties of cellulose acetate osmotic membranes, Journal of Applied Polymer Science, 9 (1965) 1341-1362.

[16] J.G. Wijmans, R.W. Baker, The solution-diffusion model: a review, Journal of Membrane Science, 107 (1995) 1-21.

[17] R.W. Baker, I. NetLibrary, Membrane technology and applications, J. Wiley, Chichester; New York, 2004.

[18] E.A. Mason, H.K. Lonsdale, Statistical-mechanical theory of membrane transport, Journal of Membrane Science, 51 (1990) 1-81.

[19] J.A. Wesselingh, A.M. Bollen, Multicomponent Diffusivities from the Free Volume Theory, Chemical Engineering Research and Design, 75 (1997) 590-602.

[20] J.A. Wesselingh, R. Krishna, Mass transfer in multicomponent mixtures, Delft University Press, Delft, Netherland, 2000.

[21] N. Stafie, D.F. Stamatialis, M. Wessling, Insight into the transport of hexane-solute systems through tailor-made composite membranes, Journal of Membrane Science, 228 (2004) 103-116.

[22] S.-U. Hong, Predicting ability of free-volume theory for solvent self-diffusion coefficients in rubbers, Journal of Applied Polymer Science, 61 (1996) 833-841.

[23] D.R. Paul, Reformulation of the solution-diffusion theory of reverse osmosis, Journal of Membrane Science, 241 (2004) 371-386.

[24] D. Fierro, N. Scharnagl, T. Emmler, A. Boschetti-de-Fierro, V. Abetz, Experimental determination of self-diffusivities through a polymer network for single components in a mixture, Journal of Membrane Science, 384 (2011) 63-71.

[25] R. Rautenbach, Membranverfahren. Grundlagen der modul- und Anlagenauslegung, Springer-Verlag, Berlin, 1997.

[26] M. Mulder, Basic principles of membrane technology, Kluwer Academic, Dordrecht; Boston, 1997.

[27] L.H. Sperling, Introduction to physical polymer science, Wiley, Hoboken, N.J., 2006.

[28] M. Roth, Solubility parameter of poly(dimethyl siloxane) as a function of temperature and chain length, Journal of Polymer Science B: Polymer Physics, 28 (1990) 2715-2719.

[29] J.E. Mark, Polymer data handbook, Oxford University Press, New York, 1999.

[30] P.J. Flory, Principles of polymer chemistry, 15. printing ed., Cornell University Press, Ithaca, 1953.

[31] J.S. Vrentas, J.L. Duda, Diffusion in polymer-solvent systems. I. Reexamination of the free-volume theory, Journal of Polymer Science B: Polymer Physics, 15 (1977) 403-416.

[32] R.J. Bearman, On Molecular Basis of Some Current Theories of Diffusion, J. Phys. Chem., 65 (1961) 1961-1968.

[33] J.L. Duda, J.S. Vrentas, S.T. Ju, H.T. Liu, Prediction of diffusion coefficients for polymer-solvent systems, 28 (1982) 279-285.

[34] T. Loflin, E. McLaughlin, Diffusion in binary liquid mixtures, The Journal of Physical Chemistry, 73 (1969) 186-190.

[35] S. Sourirajan, Reverse osmosis, Academic Press, New York, 1970.

[36] D.R. Paul, O.M. Ebra-Lima, Pressure-induced diffusion of organic liquids through highly swollen polymer membranes, Journal of Applied Polymer Science, 14 (1970) 2201-2224.

[37] D.R. Paul, J.D. Paciotti, Driving force for hydraulic and pervaporative transport in homogeneous membranes, Journal of Polymer Science: Polymer Physics Edition, 13 (1975) 1201-1214.

[38] D.R. Paul, O.M. Ebra-Lima, Hydraulic permeation of liquids through swollen polymeric networks. III. A generalized correlation, Journal of Applied Polymer Science, 19 (1975) 2759-2771.

[39] D.R. Machado, D. Hasson, R. Semiat, Effect of solvent properties on permeate flow through nanofiltration membranes. Part I: investigation of parameters affecting solvent flux, Journal of Membrane Science, 163 (1999) 93-102.

[40] D.R. Machado, D. Hasson, R. Semiat, Effect of solvent properties on permeate flow through nanofiltration membranes: Part II. Transport model, Journal of Membrane Science, 166 (2000) 63-69.

[41] T.K. Sherwood, P.L.T. Brian, R.E. Fisher, Desalination by Reverse Osmosis, Industrial & Engineering Chemistry Fundamentals, 6 (1967) 2-12.

[42] M. Soltanieh, W.N. Gill, Review of Reverse Osmosis Membranes and Transport models, Chemical Engineering Communications, 12 (1981) 279 - 363.

[43] D. Bhattacharyya, M. Williams, Introduction and Definitions - Reverse Osmosis, Van Nostrand Reinhold, New York, 1992.

[44] A.E. Yaroshchuk, Solution-diffusion-imperfection model revised, Journal of Membrane Science, 101 (1995) 83-87.

[45] D. Bhanushali, S. Kloos, C. Kurth, D. Bhattacharyya, Performance of solvent-resistant membranes for non-aqueous systems: solvent permeation results and modeling, Journal of Membrane Science, 189 (2001) 1-21.

[46] W.J. Koros, G.K. Fleming, S.M. Jordan, T.H. Kim, H.H. Hoehn, Polymeric membrane materials for solution-diffusion based permeation separations, Progress in Polymer Science, 13 (1988) 339-401.

[47] J.I. Kroschwitz, H.F. Mark, Encyclopedia of polymer science and technology, Wiley-Interscience, Hoboken, N.J., 2003.

[48] A. Conesa, S. Shen, A. Coronas, Liquid Densities, Kinematic Viscosities, and Heat Capacities of Some Ethylene Glycol Dimethyl Ethers at Temperatures from 283.15 to 423.15 K, International Journal of Thermophysics, 19 (1998) 1343-1358.

[49] K.U. Department of Chemical Engineering, Korea thermophysical properties data bank, in, Korea University, Korea.

[50] CHEM-group, Tetraethylene glycol data sheet, in.

[51] J. Kritiak, K. Kritiaková, O. Aua, P. Banduch, J. Barto, Temperature dependence of free volume distributions in polymers studied by positron lifetime spectroscopy, Le Journal de Physique IV, 03 (1993) C4-265-C264-270.

[52] B. Wang, Z.F. Wang, M. Zhang, W.H. Liu, S.J. Wang, Effect of Temperature on the Free Volume in Glassy Poly(ethylene terephthalate), Macromolecules, 35 (2002) 3993-3996.

[53] E. Habeych, A.J. van der Goot, R. Boom, Prediction of permeation fluxes of small volatile components through starch-based films, Carbohydrate Polymers, 68 (2007) 528-536.

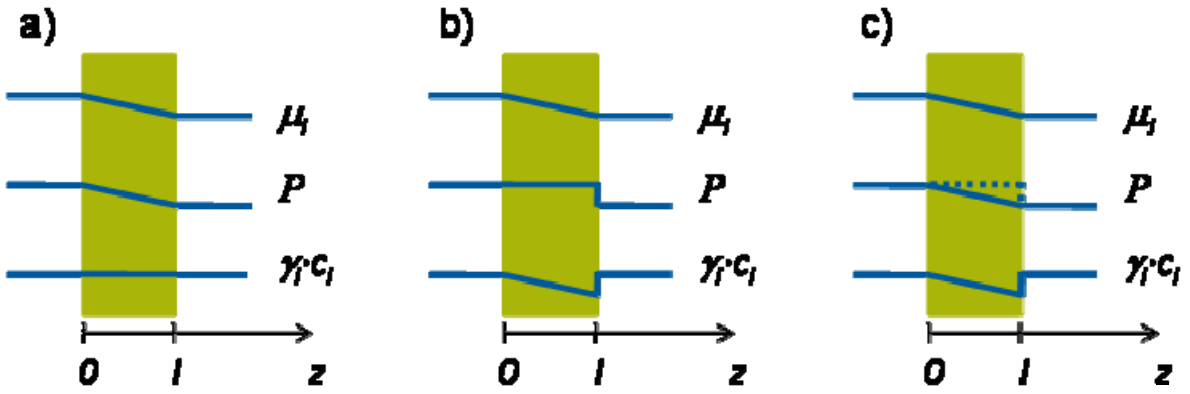

Figure 1. Pressure-driven Permeation process through a membrane, according to: a) pore–flow transport model, b) solution diffusion model, c) solution-diffusion model without constant pressure consideration.

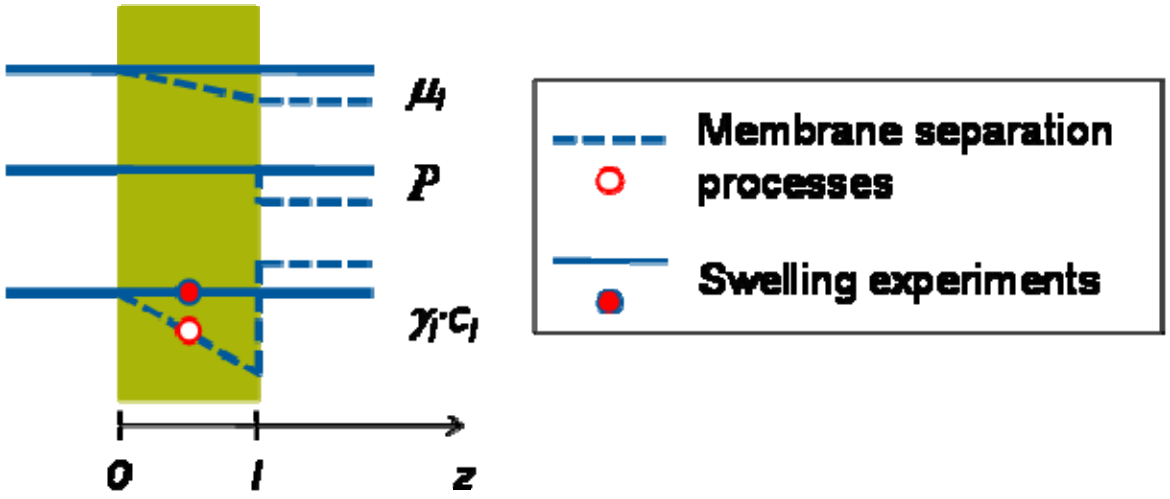

Figure 2. Schematic representation of the differences between swelling experiments and membrane separation process. The points represent the place where the solvent/solute average concentration is calculated.

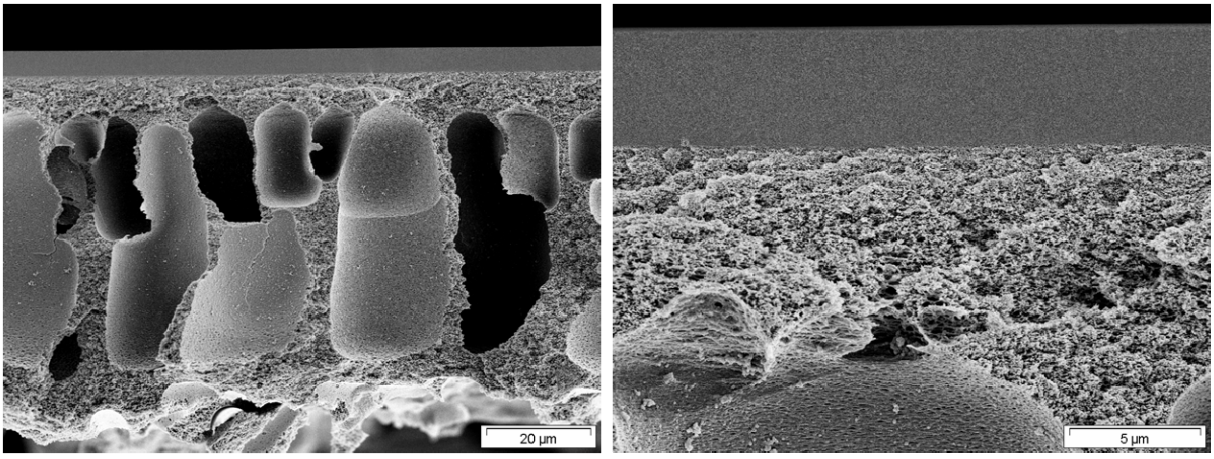

Figure 3. Scanning electron micrograph of a PDMS composite membrane.

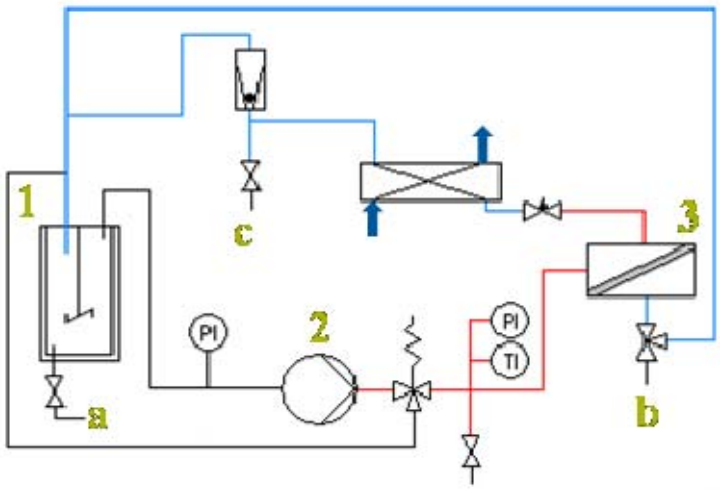

Figure 4. Schematic representation of the nanofiltration equipment. 1) supply vessel, 2) pump, 3) membrane cell, a) feed solution sample, b) permeate solution sample, c) retentate solution sample

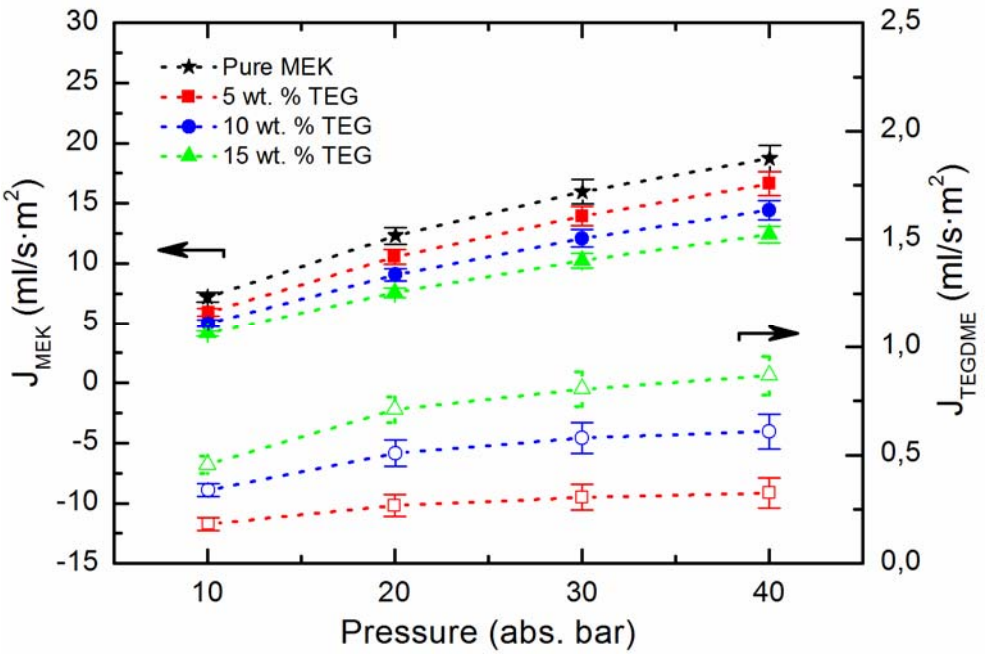

Figure 5. Experimental permeation fluxes at 25 ºC for a MEK/TEGDME system as a function of the absolute applied pressure for different TEGDME feed concentrations. The filled symbols represent the fluxes of MEK, whereas the open symbols correspond to TEGDME fluxes.

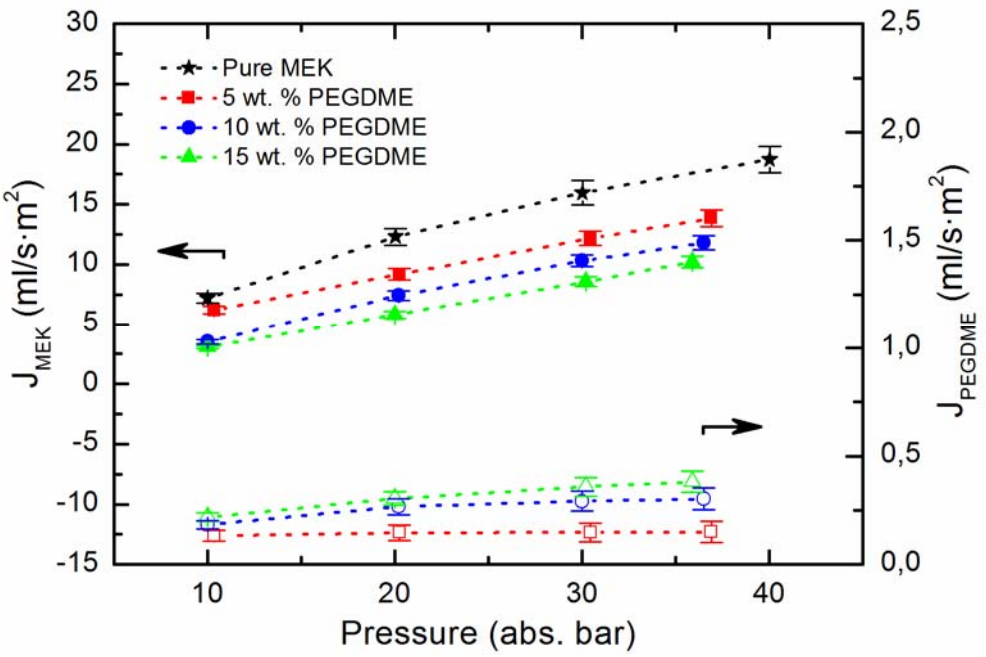

Figure 6. Experimental permeation fluxes at 25 ºC for a MEK/PEGDME system as a function of absolute applied pressure for different PEGDME feed concentrations. The filled symbols represent the fluxes of MEK, whereas the open symbols correspond to PEGDME fluxes.

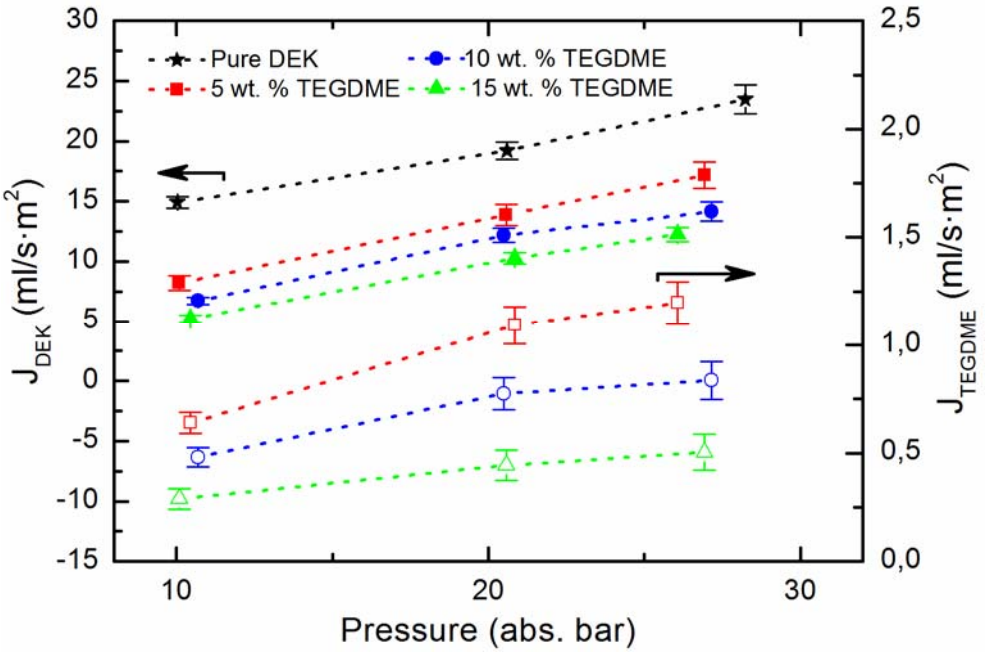

Figure 7. Experimental permeation fluxes at 25 ºC for a DEK/TEGDME system as a function of absolute applied pressure for different TEGDME feed concentrations. The filled symbols represent the fluxes of DEK, whereas the open symbols correspond to TEGDME fluxes.

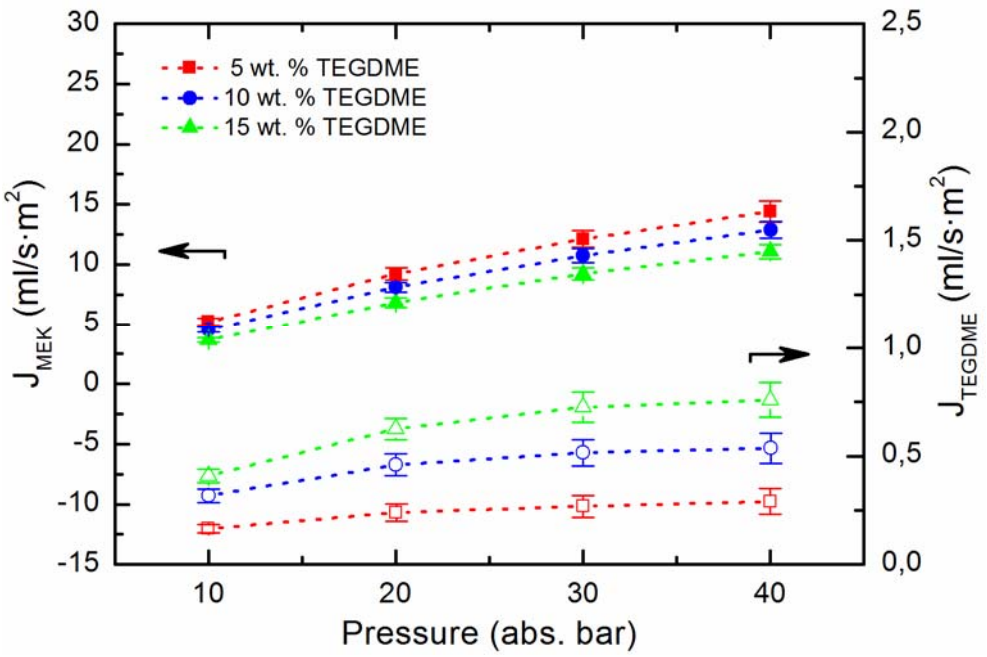

Figure 8. Experimental permeation fluxes at 20 ºC for a MEK/TEGDME system as a function of absolute applied pressure for different TEGDME feed concentrations. The filled symbols represent the fluxes of MEK, whereas the open symbols correspond to TEGDME fluxes.

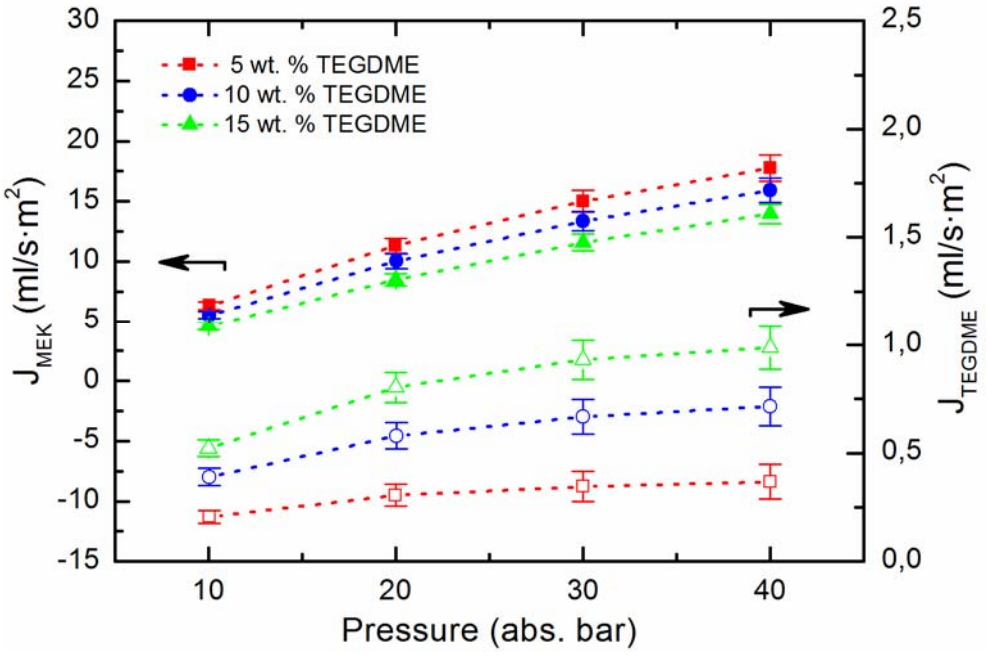

Figure 9. Experimental permeation fluxes at 30 ºC for a MEK/TEGDME system as a function of absolute applied pressure for different TEGDME feed concentrations. The filled symbols represent the fluxes of MEK, whereas the open symbols correspond to TEGDME fluxes.

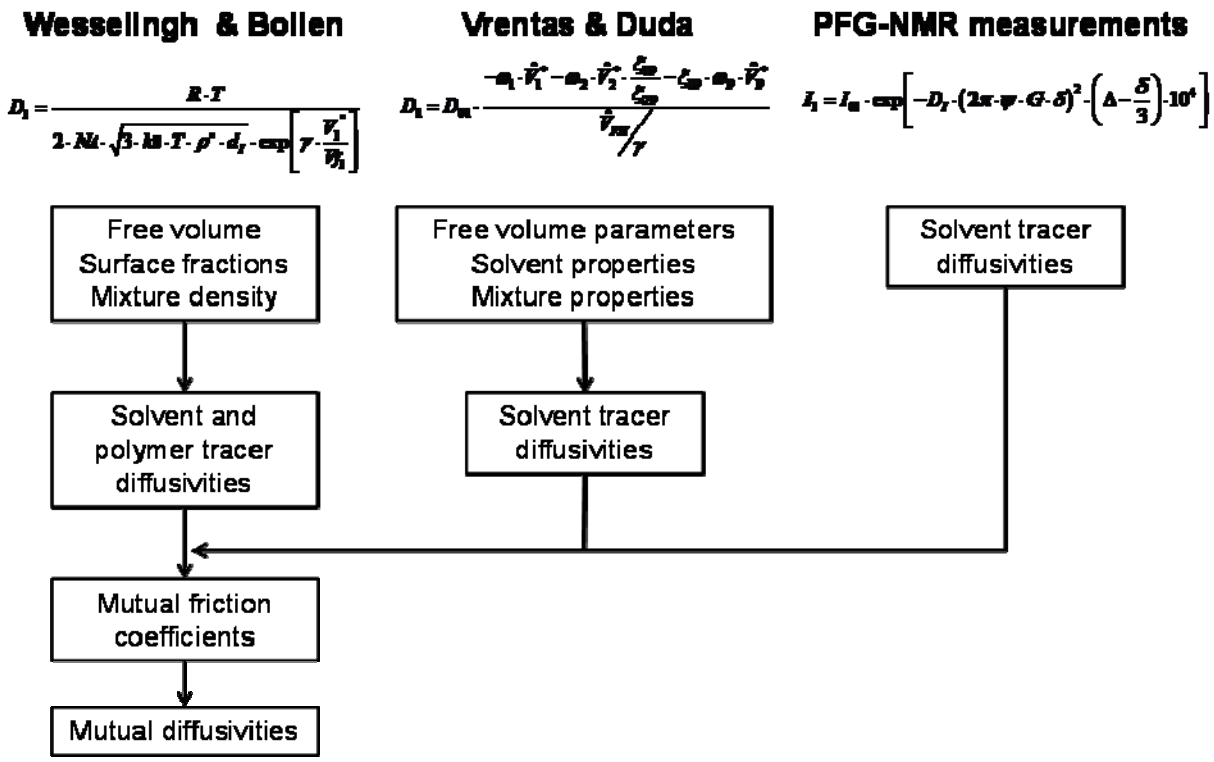

Figure 10. Scheme of different calculation methods for the estimation of mutual diffusion coefficients.

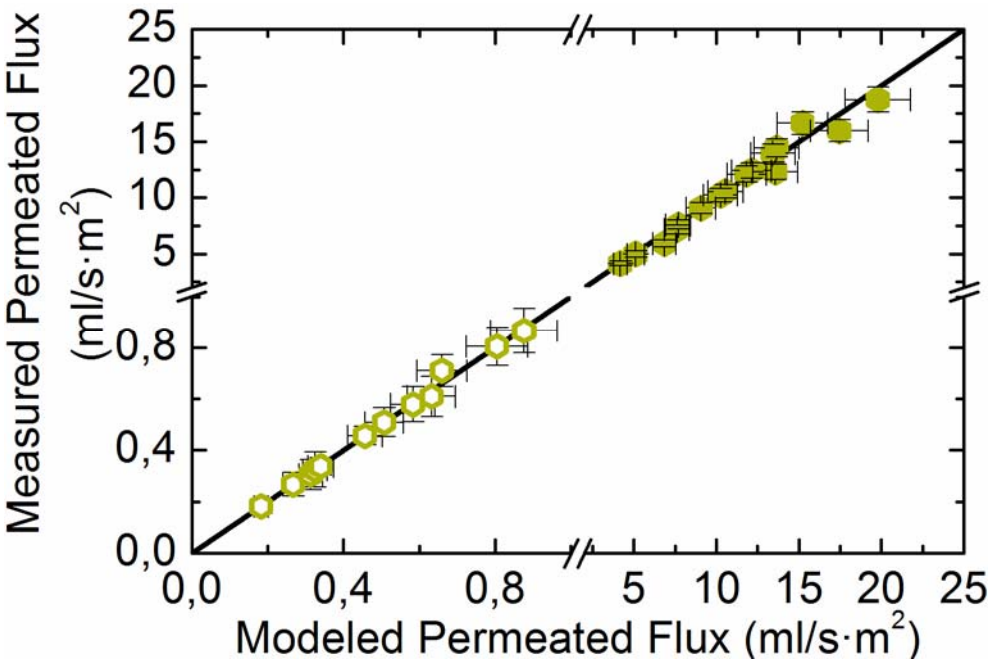

Figure 11. Correlation between measured MEK/TEGDME permeation fluxes and simulated data calculated by the solution-diffusion with imperfections model. The filled symbols represent the fluxes of MEK, whereas the open symbols correspond to TEGDME fluxes.

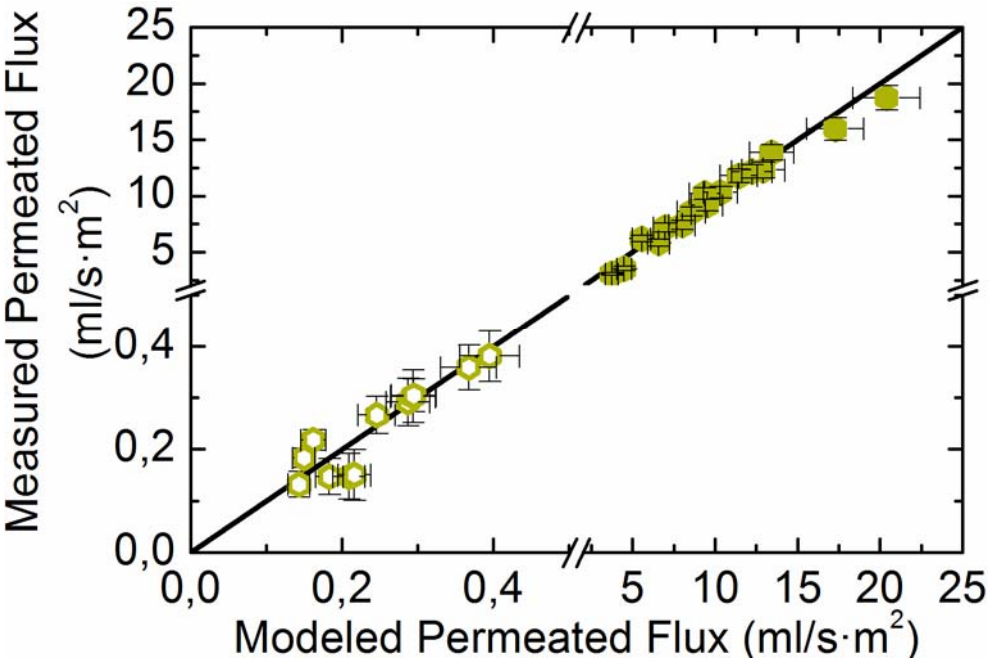

Figure 12. Correlation between measured MEK/PEGDME permeation fluxes and simulated data calculated by the solution-diffusion with imperfections model. The filled symbols represent the fluxes of MEK, whereas the open symbols correspond to PEGDME fluxes.

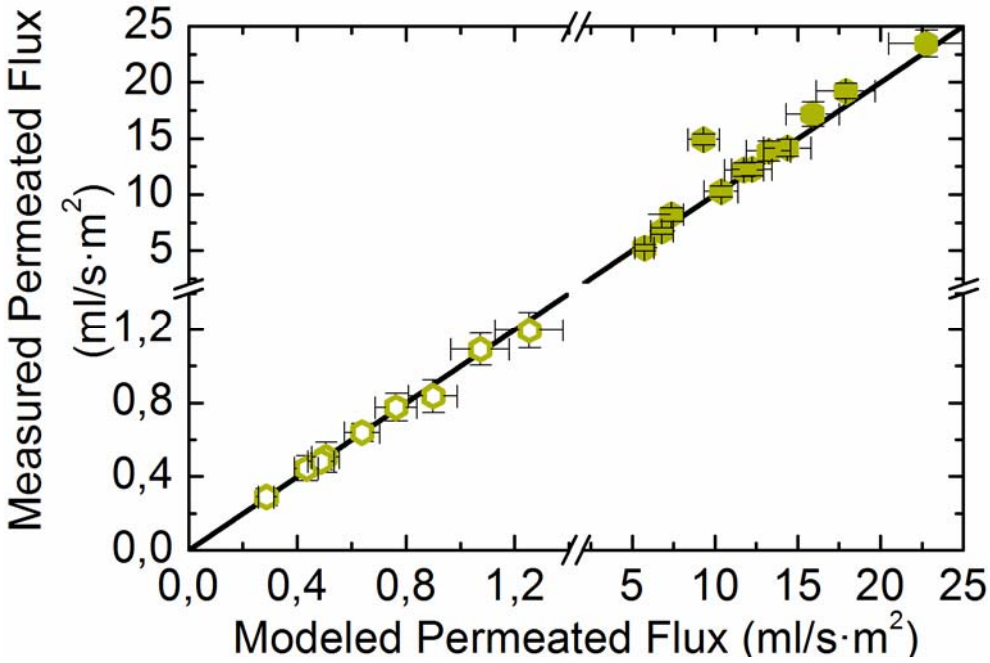

Figure 13. Correlation between measured DEK/TEGDME permeation fluxes and simulated data calculated by the solution-diffusion with imperfections model. The filled symbols represent the fluxes of DEK, whereas the open symbols correspond to TEGDME fluxes.

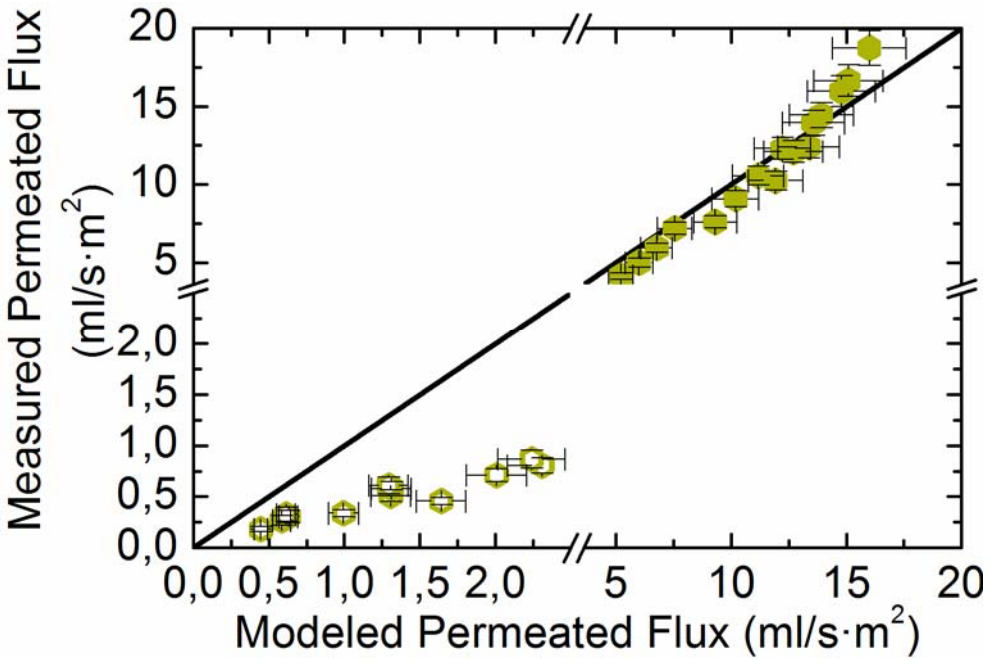

Figure 14. Correlation between measured MEK/TEGME permeation fluxes and simulated data calculated by the solution-diffusion with imperfections model, with permeant concentrations estimated by interaction parameters from binary systems. The filled symbols represent the fluxes of MEK, whereas the open symbols correspond to TEGDME fluxes.